Korean J. Chem. Eng., 39(10), 2664-2674 (2022)
DOI: 10.1007/s11814-022-1133-0

pISSN: 0256-1115
eISSN: 1975-7220

Construction of superhydrophilic and underwater superoleophobic corn stalk/konjac glucomannan aerogel for high-efficiency oil/water emulsion separation

Wenfeng Wang*, Lu Mou*, Di Yang*, Yuanhao Wang*,,†, and Fan Yang****

*School of Light Industry and Chemical Engineering, Dalian Polytechnic University, Dalian, 116034, China
**Xiamen Institute of Rare Earth Materials, Haixi Institute, Chinese Academy of Sciences, Xiamen, 361026, China
(*Received 12 December 2021 • Revised 23 March 2022 • Accepted 2 April 2022*)

Abstract−An anti-fouling aerogel with superior separation performance for separation of oil/water emulsion is of great significance to industrial development due to continuously increasing oily industrial wastewater. Herein, a superhydrophilic/underwater superoleophobic porous biobased aerogel with a three-dimensional network structure was prepared by the agricultural waste corn stalk (CS) incorporated with konjac glucomannan (KGM) through simple sol-gel and freeze-drying methods. The oil/water separation mechanisms and the effect of aerogel structural changes on the separation performance of CS/KGM aerogel for oil-in-water emulsions are discussed in detail. Using toluene as an oil phase, $CS_{3.50}K_{1.25}$ exhibited outstanding separation performance with an excellent separation efficiency above 96.26% and a high permeate flux above 2,381 L m^{-2} h^{-1} for oil-in-water emulsions. As expected, the separation efficiency and permeation flux can be wholly recovered after washing, indicating the aerogel possesses good sustainability. Moreover, CS/KGM aerogel has the advantages of low cost, simple preparation, eco-friendly and anti-fouling, revealing a promising candidate for the treatment of oily wastewater pollution.

Keywords: Aerogel, Waste Corn Stalk, Underwater Superoleophobicity, Antifouling Property, Oil/water Separation

INTRODUCTION

With the rapid development of industry and the continuous expansion of production scale, the discharge of oily wastewater has posed a great threat to the ecological environment and human health, which makes oil/water separation a worldwide problem [1-3]. To address this problem, various methods have been developed for efficient separation of oil/water mixtures, including centrifugation [4], flotation [5], in-situ burning [6] and adsorption [7]. However, most of these methods are not suitable to separate oil-in-water emulsions, especially those emulsions stabilized by surfactants [8]. The oil droplet size of the surfactant-stabilized emulsion is generally less than 20 μm [9], which is not easy to demulsify and coalesce. In addition, the presence of surfactants will reduce oil/water interfacial tension, making oil-in-water emulsions in a relatively stable state [10]. Therefore, the separation of surfactant-stabilized emulsions is still a huge challenge [11].

Physical filtration is a suitable method for oil-in-water emulsion separation, which is usually based on separation materials with special wettability (superhydrophobicity and superhydrophilicity/underwater superoleophobicity, etc.) [12]. Currently, superhydrophilic/underwater superoleophobic membranes have received extensive attention due to their distinct advantages, including low energy consumption, flexible and low environmental pollution [13]. Cui et al. [1] prepared a polyacrylamide nanofiber membrane with an irregular rod-like structure through atom transfer radical polymerization, and it could separate oil/water emulsions effectively. Zhu et al. [14] fabricated a superhydrophilic/underwater superoleophobic SSM mesh with rough surface structures via a facile strategy for efficient separation of oil/water emulsions. However, most membranes with special wettability are prepared by surface engineering [15], which may suffer mechanical damage and lose their superoleophobicity after long-term washing. Meanwhile, these membranes usually show thin 2D structures with short permeation channels and low porosity, which is not helpful for high-efficiency oil/water separation [16]. Considering the disadvantages of 2D membranes, 3D porous materials (sponge [17] and aerogel [18,19], etc.) with high porosity have emerged as an alternative strategy for realizing emulsion separation. Even so, the practical applications of most 3D porous materials with underwater superoleophobicity are still limited by relatively complicated preparation processes and expensive raw materials [20]. The treatment requirements of actual oily wastewater have prompted people to develop more novel oil/water separation materials with low cost and simple preparation methods.

Konjac glucomannan (KGM) is an abundant natural biomacromolecule derived from the tuber of konjac plant with hydrophilicity [21]. It produces a thermally irreversible gel in the presence of an alkaline coagulant, making it a good framework material for preparing aerogel [22]. KGM-based aerogels have been widely studied for many different applications, including adsorption [23], thermal insulation [24] and electronic devices [25] with interesting properties. However, there are few reports about the application of KGM-based aerogels in oil/water emulsion separation. It is beneficial for developping more high-value products of KGM to develop the separation performance for oil/water emulsions of KGM-based aerogels. On the other hand, corn stalk (CS) is an abundant agricultural

†To whom correspondence should be addressed.
E-mail: yuanhaowang@126.com

waste, mainly composed of cellulose, hemicellulose and lignin [26]. Nevertheless, most of the CS is thrown away or burned because of low utilization, which releases a large amount of PMs and gaseous pollutants to the environment [27]. More and more researchers incorporate it into material matrices to prepare composites due to its biodegradability, low cost and preferable mechanical properties [28,29]. Jiang et al. [30] developed a novel porous composite sponge by modifying chitin with corn stalk and AgNPs for medical hemostasis. The results showed that the introduction of corn stalk improved the structure, water absorption capability and mechanical properties of the sponge. The preparation of CS composites not only endows materials with cost-effectiveness, but also provides an effective way to eliminate environmental pollution caused by excess agricultural waste.

In this work, a novel CS/KGM aerogel for oil/water emulsion separation was prepared via a simple freeze-drying process. Hydrophilic KGM was used to construct the framework of aerogel through chemical cross-linking and CS was used to improve the surface roughness and porous structure of KGM aerogel [31]. The obtained CS/KGM aerogel shows the high flux and separation efficiency for surfactant-stabilized oil-in-water emulsion separation, and this work could greatly promote the development of oil/water separation materials in practical applications.

MATERIALS AND METHODS

1. Materials

KGM was purchased from Hubei Johnson Konjac Technology Co., Ltd., China. CS was obtained from Local farmers in Dalian, after cutting it into small pieces and washing, CS was dried at 80 °C to a constant weight. The dried CS was pulverized into powder and sieved through a 200-mesh Tyler sieve (aperture 74 μm) before use. Anhydrous sodium carbonate (Na_2CO_3) was purchased from Shenyang Xindong Reagent Co., Ltd., China. Other reagents and solvents were of analytical grade and purchased from Sinopharm Chemical Reagents. All solutions were prepared with deionized water.

2. Preparation of CS/KGM Aerogel

The CS/KGM aerogel was prepared by sol-gel and freeze-drying methods. Na_2CO_3 (0.4%, w/v) and KGM (0.5-1.5%, w/v) were added into deionized water (100 mL) at room temperature and stirred for 2 h to obtain a uniform mixed solution. Then, CS (0-5%, w/v) was added to the mixed sol and stirred for 30 min to obtain a homogeneous mixture. The mixture was poured into the mold and reacted at 95 °C for 1.5 h to obtain CS/KGM hydrogels. After cooling to room temperature, CS/KGM hydrogels were pre-frozen at −20 °C for 12 h. The pre-frozen samples were placed in a freeze dryer and dried at −60 °C for 24 h to obtain CS/KGM aerogels (SCIENTZ-10N, China). All the aerogels were signed CS_xK_y (CS and K represent corn stalk and konjac glucomannan respectively, x and y after CS and K represent the mass percentage of the substance in the original solution composition). The preparation process of CS/KGM aerogel and its application in oil/water separation is illustrated in Scheme 1.

3. Characterization of CS/KGM Aerogel

The surface morphologies of the CS/KGM aerogels were observed using a scanning electron microscope (SEM) (JSM-7800F, JEOL, Japan) with an acceleration voltage of 5 kV. Before observation, the aerogels were cut into flat pieces with a blade and then coated with gold particles. FT-IR spectra were conducted to analyze the chemical structures of CS/KGM aerogels by an infrared spectrometer (Spectrum Two, PerkinElmer, USA) in the range of 4,000-500 cm^{-1} in KBr pellets. The structural and phase analysis of CS/KGM aerogel was investigated using an X-ray diffractometer (XRD-7000S, Shimadzu, Japan) with Cu Kα radiation at 40 kV and 30 mA in the range of 10-70 at room temperature. TGA was carried out to determine the thermostability of CS/KGM aerogels with a TG 209 analyzer (Netzsch, Selb, Germany). The specimen was

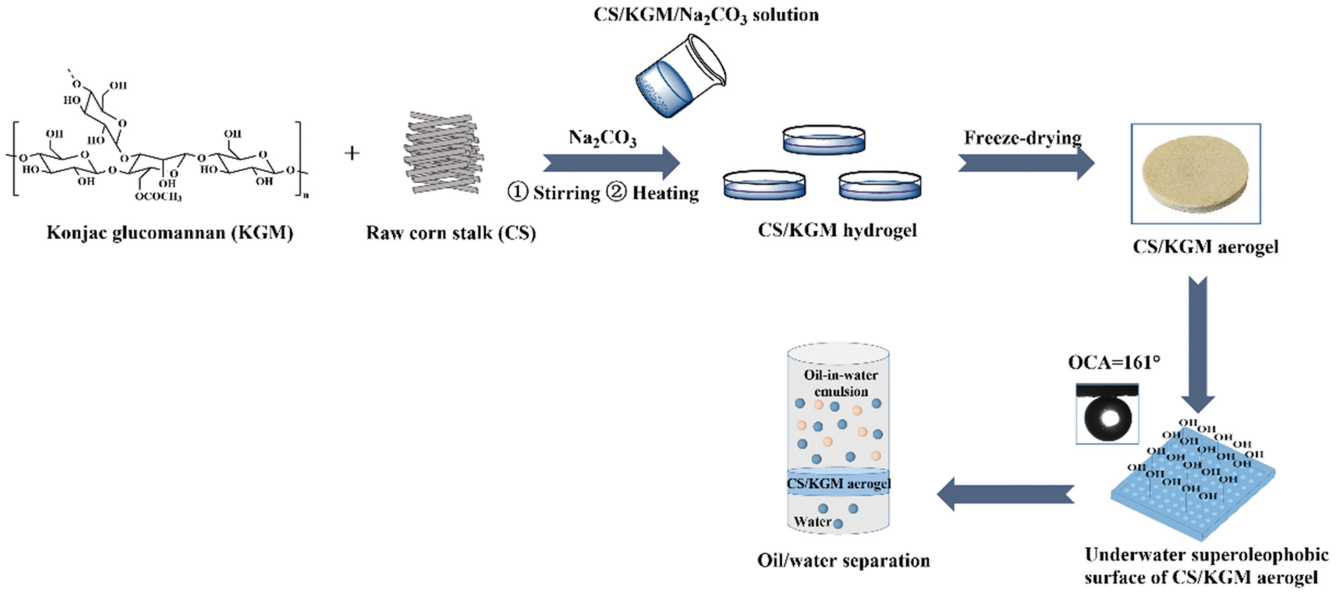

Scheme 1. The preparation of CS/KGM aerogel and its application in oil/water separation.

heated from 30 °C to 600 °C at heating rate 10 °C/min, and weight loss curve was recorded. All measurements of water contact angle (WCA) and underwater oil contact angles (UOCAs) of CS/KGM aerogel were conducted using contact angle equipment (JC2000D5H, Shanghai Zhongchen Digital Technology Equipment Co., Ltd., China) at room temperature. The change of the size distribution between pristine emulsion and filtrate was observed through an optical microscope (DS-Fi1, NIKON, Japan) and a dynamic light scattering (DLS) (BI-200SM/BI-9000, Brookhaven, USA).

4. Separation of Oil-in-water Emulsion

Surfactant-free oil-in-water emulsion was prepared by mixing toluene and water at a ratio of 1 : 100 (v/v) and then sonicating the mixture for 20 minutes [1]. The surfactant-stabilized oil-in-water emulsion was also prepared by the above method, except by adding the surfactant sodium dodecyl sulfate (SDS) with a concentration of 0.5 mg/mL.

The CS/KGM aerogel was pre-wetted with water (effective separation area of 12.56 cm^2), then the prepared oil-in-water emulsion was separated through the vacuum filter device equipped with CS/KGM aerogel at 0.09 MPa and 25 °C. After the separation, the CS/KGM aerogel was washed with deionized water for the next cycle of the oil/water separation performance. The concentration of toluene before and after separation was measured by the standard curve method [18]. The prepared emulsion is diluted into toluene-water solutions of different concentrations, and the linear relationship between the concentration of toluene in the solution and the absorbance is established by an ultraviolet-visible spectrophotometer at 261 nm. The calculation of the separation efficiency R (%) in the oil-water emulsion separation process is shown in Eq. (1) [32].

$$R = \left(1 - \frac{C_p}{C_0}\right) \times 100\% \quad (1)$$

where C_0 and C_p are the toluene concentration in the initial emulsion and the filtrate, respectively.

The permeation flux of CS/KGM aerogel in the oil-in-water emulsion separation process is calculated by the volume of the filtrate per unit time (L m^{-2} h^{-1}), as shown in Eq. (2) [18].

$$F = \frac{V}{At} \quad (2)$$

where V is the volume of the oil-in-water emulsion, A is the effective separation area of the CS/KGM aerogel, and t is the penetration time.

RESULTS AND DISCUSSION

1. Morphology and Composition Analysis

Fig. 1 shows the surface morphological of CS/KGM aerogels. As shown in Fig. 1(a), although $CS_0K_{1.25}$ has a large number of microporous structures, they were collapsed and stacked after being wetted by water. This is because the mechanical properties of the skeleton structure constructed by pure KGM are poor and cannot resist the extreme capillary force generated when water penetrates through the aerogel [33]. The disappearance of the porous structure is not

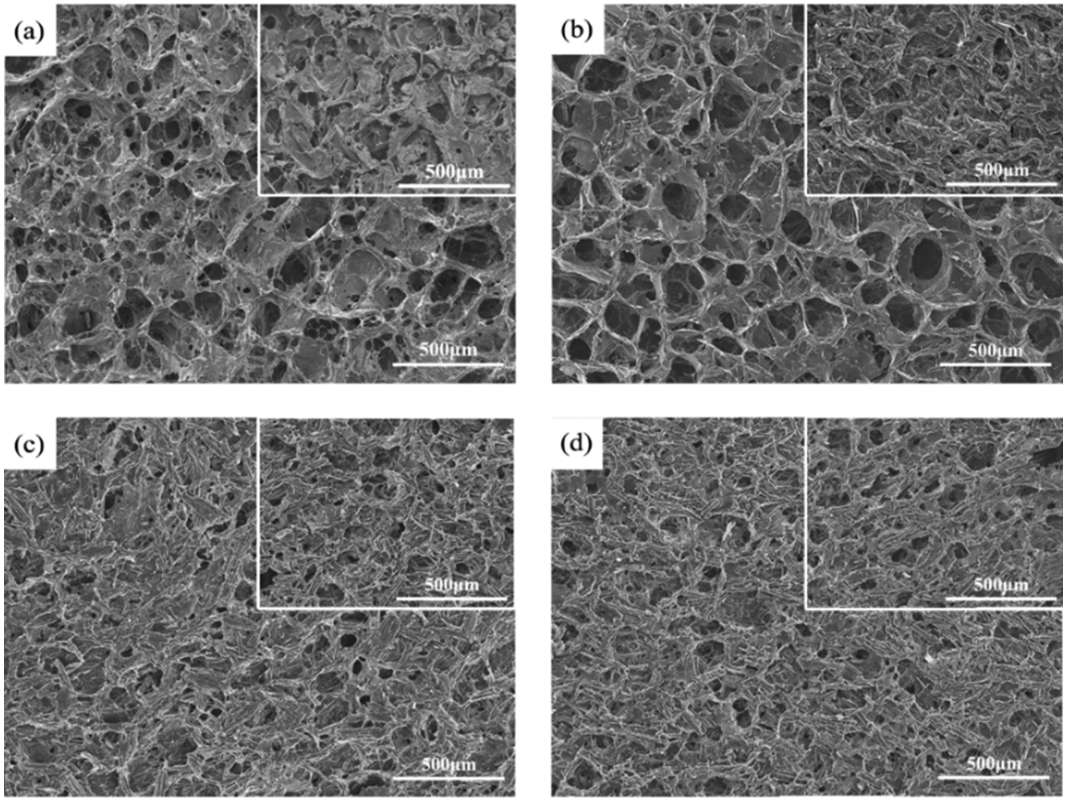

Fig. 1. SEM images of CS/KGM aerogels: (a) $CS_0K_{1.25}$, (b) $CS_{2.00}K_{1.25}$, (c) $CS_{3.50}K_{1.25}$, (d) $CS_{5.00}K_{1.25}$. The insets were corresponding aerogels after being wetted by water.

conducive to the penetration of water during the oil-in-water emulsion separation process. As shown in Fig. 1(b), the surface structure of $CS_{2.00}K_{1.25}$ did not change significantly after adding CS, but the structure collapse phenomenon was slightly improved after being wetted by water. It is because the addition of CS leads to the shape of the ice crystals formed during the freezing process, which affects the shape of the porous network of aerogel [31]. Meantime, the structure of the aerogel can be supported and bridged by CS, which improves the strength of the skeleton. When the CS amount increased to 3.50% (Fig. 1(c)), the pore size of the $CS_{3.50}K_{1.25}$ was significantly reduced and the surface roughness was maintained better due to the existence of corn stalk when the surface wetted with water, which is beneficial to the demulsification of the oil-in-water emulsion. More importantly, the collapse phenomenon of the aerogel was significantly improved after being wetted by water, and it maintained rich porous structures, which is conducive to water penetration. With a further increase of CS amount, the surface morphology of the aerogel showed no apparent change (Fig. 1(d)). The results indicate that the incorporation of CS can improve the skeleton strength of the aerogel, and it can resist the destruction of capillary force generated during the separation process. Therefore, the porosity of the aerogel was significantly enhanced with the addition of CS [34].

Fig. 2 shows the FT-IR spectra of CS, KGM, $CS_0K_{1.25}$ and $CS_{3.50}K_{1.25}$. The absorption peaks at 3,420 cm^{-1} and 2,878 cm^{-1} are attributed to the stretching vibration of O-H and the C-H group of methyl. The peak at 1,732 cm^{-1} was related to the C=O stretching of the acetyl group [35]. The peaks at about 872 and 807 cm^{-1} were related to the mannose in KGM [36,37]. Compared with KGM, the absorption peaks of $CS_0K_{1.25}$ at 1,732 cm^{-1} almost completely disappeared because of the deacetylation reaction of KGM molecules under alkaline heat conditions to form irreversible gels [38,39]. Similar to the effect on KGM and agar [35], deacetylation is also conducive to enhancing the hydrogen bond between KGM and CS. The partial removal of acetyl groups of KGM could induce associations between the acetyl-free regions of KGM chains and CS via hydrogen bonding. These made the accumulation of molecular segments more compact, resulting in enhancing the mechanical properties

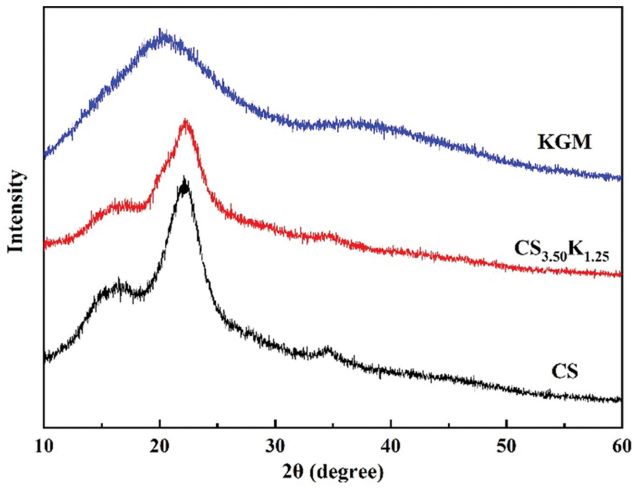

Fig. 3. XRD spectra of CS, KGM and $CS_{3.50}K_{1.25}$.

of the CS/KGM aerogel. Also, the increased amount of free -OH groups allowed more sites for water sorption and it is benefit to the hydrophilic properties of the aerogel. Due to hemicellulose and lignin existing, the absorption of the C=O and ester groups peaks at 1,742 cm^{-1} and 1,245 cm^{-1} [40], the absorption peaks at 1,742 cm^{-1} and 1,245 cm^{-1} once more appear in the FT-IR spectra of $CS_{3.50}K_{1.25}$.

The XRD patterns of KGM, CS and $CS_{3.50}K_{1.25}$ are shown in Fig. 3. The peak at 2θ=20.61° indicates the KGM molecule exists in a nearly amorphous structure [41,42]. The characteristic peaks of the cellulose type I structure appeared at 2θ=15.4°, 22.1° and 34.5° in the structure of CS [43]. After Na_2CO_3 was added and heated, the diffraction peaks at 2θ=15.4°, 22.1° and 34.5° indicate that the crystal structure of CS cellulose was not destroyed. The XRD patterns and FT-IR spectra consistently show that CS mainly participates in the formation of CS/KGM aerogel through a physical blending of CS cellulose. Furthermore, the KGM/CS aerogel did not show a new derivative peak compared to the KGM and CS, indicating a high degree of compatibility of CS in the KGM/CS aerogel.

The thermal stability of the prepared $CS_0K_{1.25}$ and $CS_{3.50}K_{1.25}$ was evaluated (Fig. 4). The first stage mass loss of ~5% at around

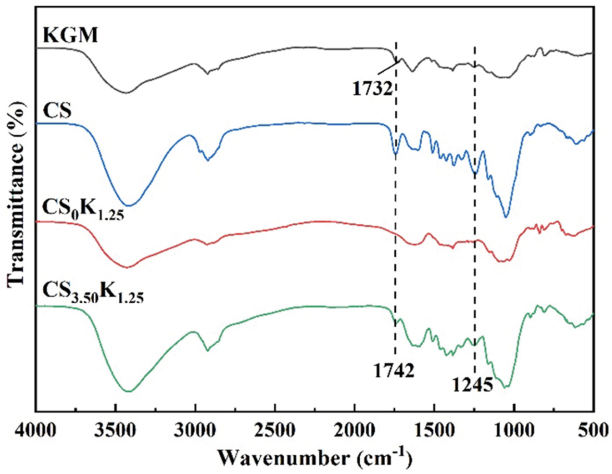

Fig. 2. FT-IR spectra of CS, KGM, $CS_0K_{1.25}$ and $CS_{3.50}K_{1.25}$.

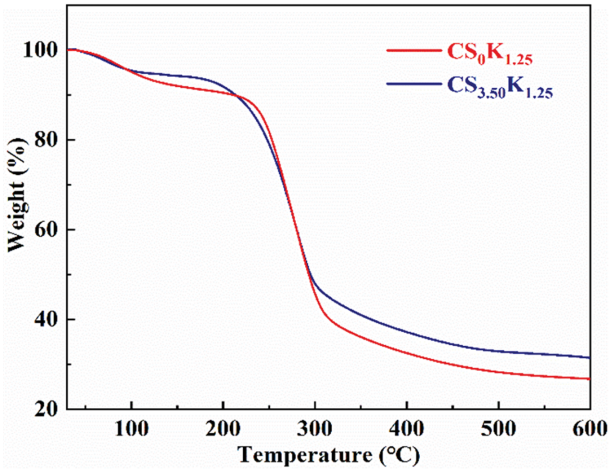

Fig. 4. TGA curve of $CS_0K_{1.25}$ and $CS_{3.50}K_{1.25}$.

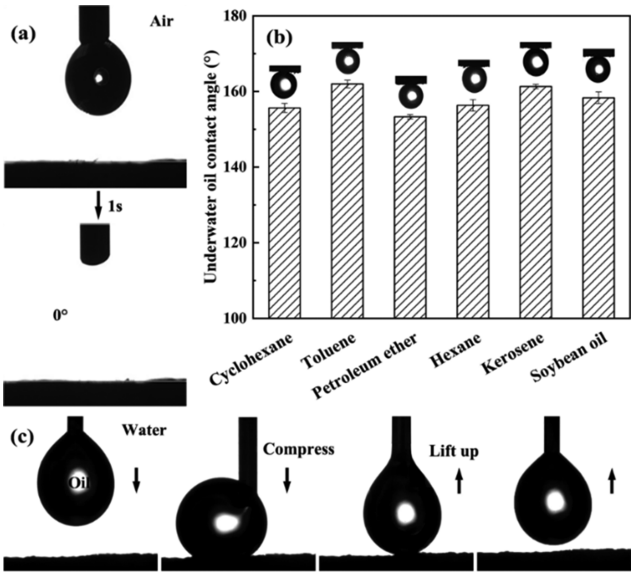

Fig. 5. The wettability of $CS_{3.50}K_{1.25}$ ((a) water contact angle; (b) various underwater oil contact angle; (c) underwater oil adhesion property).

100 °C was due to the desorption of adsorbed water in the structure, which is independent of the thermal stability of $CS_{3.50}K_{1.25}$ [27]. The second stage of mass loss from 236.83 °C to 315.10 °C was attributed to the pyrolysis of polysaccharide [31], where about 62% of weight was lost. Compared with the $CS_0K_{1.25}$, the weight loss rate of $CS_{3.50}K_{1.25}$ was reduced, indicating that the addition of CS could improve the thermal stability of the aerogel.

2. Determination of Wettability

To investigate the wettability of the CS/KGM aerogel surface, the water contact angle (WCA) in the air and the underwater oil contact angle (UWCA) of $CS_{3.50}K_{1.25}$ were evaluated. As shown in Fig. 5(a), since the aerogel surface contains a large number of hydrophilic groups, the water droplet wetted and spread rapidly on its surface within 1 s (WCA≈0°), indicating the superhydrophilicity. All of the UWCA of the aerogel (Fig. 5(b)) were higher than 150° (especially for toluene, the UWCA is 161°), indicating the superior underwater superoleophobicity of the aerogel. It is generally believed that the underwater superoleophobicity of materials depends on the surface hydrophilic groups and the roughness structure [44]. A large number of hydrophilic hydroxyl groups on the aerogel surface interacted with water to form a hydrated layer on the rough surface, resulting in oil droplets being suspended in the Cassie-Baxter regime [45,46]. According to the Cassie-Baxter model [47,48], the effective contacting area of oil droplet with the aerogel surface is sharply reduced after the formation of the hydration layer, which explains the high UWCA of the aerogel. Additionally, the oil (dichloromethane) adhesive behavior was also analyzed in Fig. 5(c). It was observed that when dichloromethane droplet contact with the aerogel surface under pressure, no significant deformation during lifting up oil droplet, which indicating the low oil adhesion property of aerogel.

3. Oil/Water Separation for Oil-in-water Emulsion

Fig. 6 shows the possible mechanisms in the separation process of $CS_{3.50}K_{1.25}$ for surfactant-free emulsion and surfactant-stabilized emulsion. During the separation of surfactant-free emulsion (Fig. 6(a)), water molecules combined with the hydroxyl groups on the surface of the aerogel through hydrogen bonds to form a hydration layer and spread quickly on the surface of the aerogel. Then water penetrated hydrophilic aerogel through the porous structure. The oil droplets are first intercepted by the aerogel surface with micro/nanoporous structures based on the size-sieving effect [49]. Due to the driving of the hydraulic power and the superoleophobicity of the aerogel surface, the oil droplets freely rolled and coalesced on the aerogel surface [50]. After that, the oil droplets are released and lifted under the action of buoyancy to form an oil layer on the

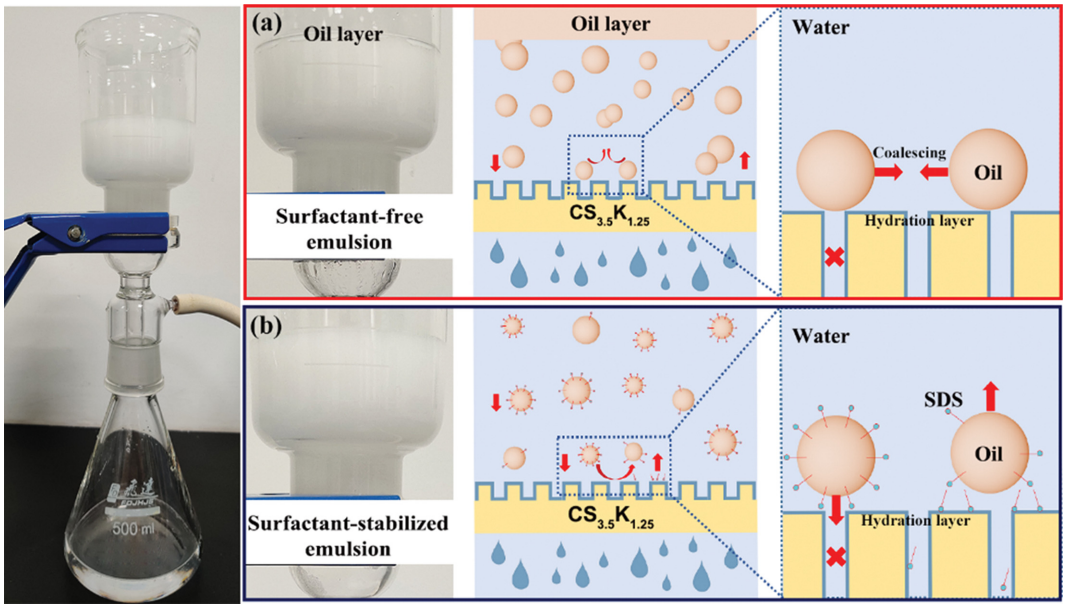

Fig. 6. The oil-in-water emulsion separation process and illustrations of $CS_{3.50}K_{1.25}$: (a) surfactant-free emulsion; (b) surfactant-stabilized emulsion.

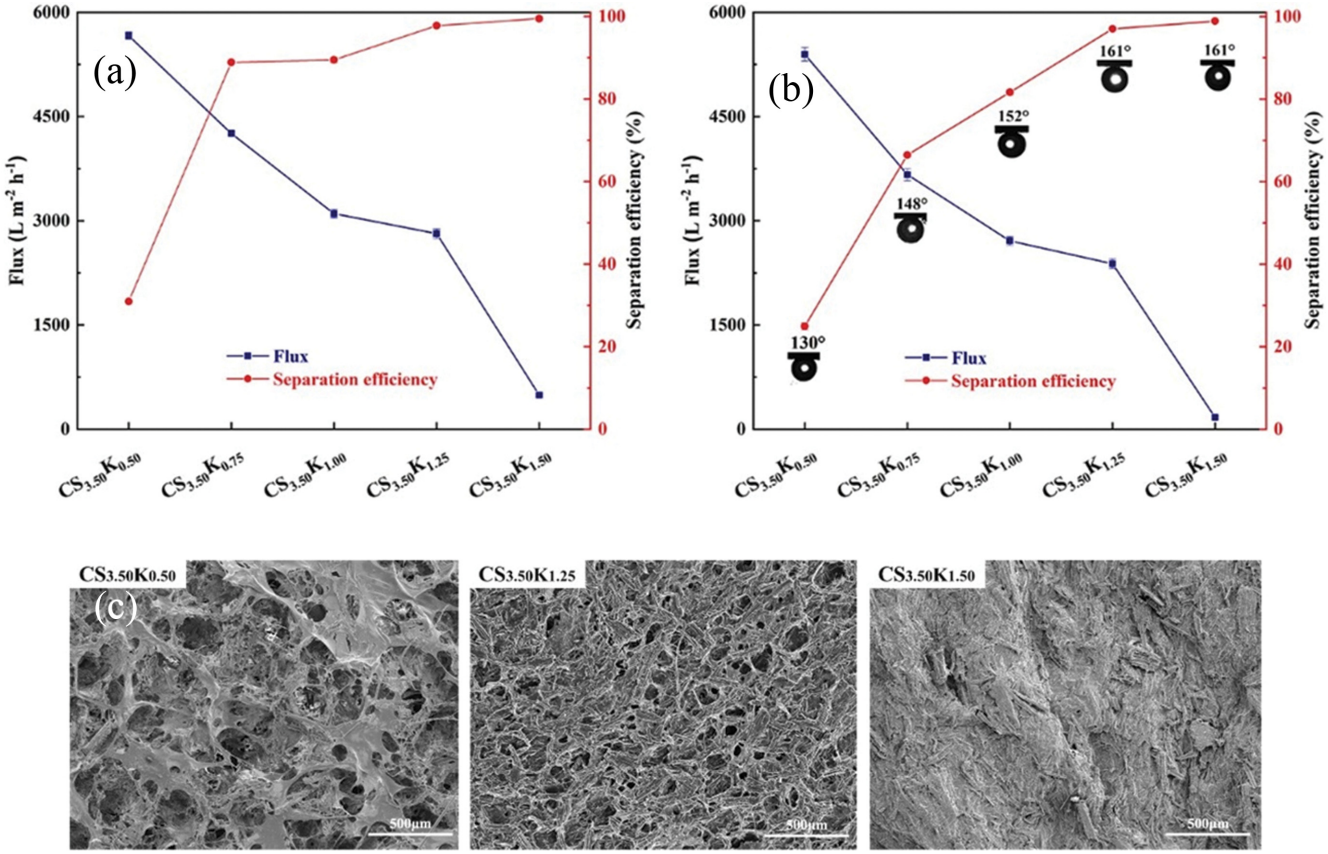

Fig. 7. Separation performance of CS/KGM aerogel for oil-in-water emulsion ((a) surfactant-free emulsion; (b) surfactant-stabilized emulsion.) and the SEM images (c) with different KGM content.

surface of the water [45,50]. During the separation of surfactant-stabilized emulsion (Fig. 6(b)), a large number of hydroxyl groups on the aerogel surface combined with the water molecules around the oil droplets via hydrogen bonds to destroy the stability of the emulsion [45]. Besides, it also facilitated the capture of the hydrophilic groups of the surfactants, resulting in the breakdown of the surfactant layer of the oil droplets [51]. The thermodynamic equilibrium was broken with the partial removal and rearrangement of the surfactant on the oil droplet surface [52]. Consequently, the stable emulsion droplets were demulsified and coalesced on the aerogel surface. The following oil-water separation process is similar to that of a stable oil-water system without surfactant. Compared with the separation processes of surfactant-free emulsion, a filter cake formed by surfactants and oil droplets on the surface of the aerogel will cause a decrease in flux [50].

Fig. 7 shows the effect of different KGM content on the separation performance of CS/KGM aerogels for surfactant-free emulsion and surfactant-stabilized emulsion. The presence of KGM will make the aerogel have porosity and superhydrophilic properties, but the micro/nanoporous structure will collapse and stack if excessive KGM exists (Fig. 7(c)). This makes the excessive KGM content not conducive to maintaining the porous structure of CS/KGM aerogel, resulting in a decrease in flux. Therefore, the flux decreased from 5,700 L m^{-2} h^{-1} to 200 L m^{-2} h^{-1} (Fig. 7(a)) as the content of KGM increased from 0.50% to 1.50%. Compared with the flux of surfactant-free emulsion, the flux of surfactant-stabilized emulsion was slightly decreased because the pores that existed in the aerogel were blocked by the surfactant during the separation process (Fig. 7(b)) [53]. It is different from the effect of KGM content on the flux that the separation efficiency increases with the increase of KGM content. First, the increase of KGM content is beneficial to improving the hydrophilic property of the aerogel. This is a benefit to enhancing the interaction between surfactants and aerogel and a better demulsification process occurs. Consequently, the oil droplet is released and lifted by the buoyancy [45]. Secondly, the water droplets adsorbed by the aerogel can accumulate, a handicap to prevent the oil droplets from touching the surface of the aerogel [54], thus improving the performance of oil/water separation. With the increase of KGM content, the hydrophilic hydroxyl groups of aerogel bonded more H_2O [55], which played an essential role in the formation of the hydrated layer [56], improving the underwater superoleophobicity [57]. Therefore, the separation efficiency of the aerogel for the oil-in-water emulsion can be improved with the increase of KGM content.

The effect of different CS content on the separation performance of CS/KGM aerogels was also investigated, as shown in Fig. 8. The incorporation of CS is beneficial to enhancing the porous structure of aerogel and increasing their porosity [58], thereby increasing the flux. Hence, the flux of the aerogel for surfactant-free emulsion separation increased from 1,060 L m^{-2} h^{-1} to 4,600 L m^{-2} h^{-1} with

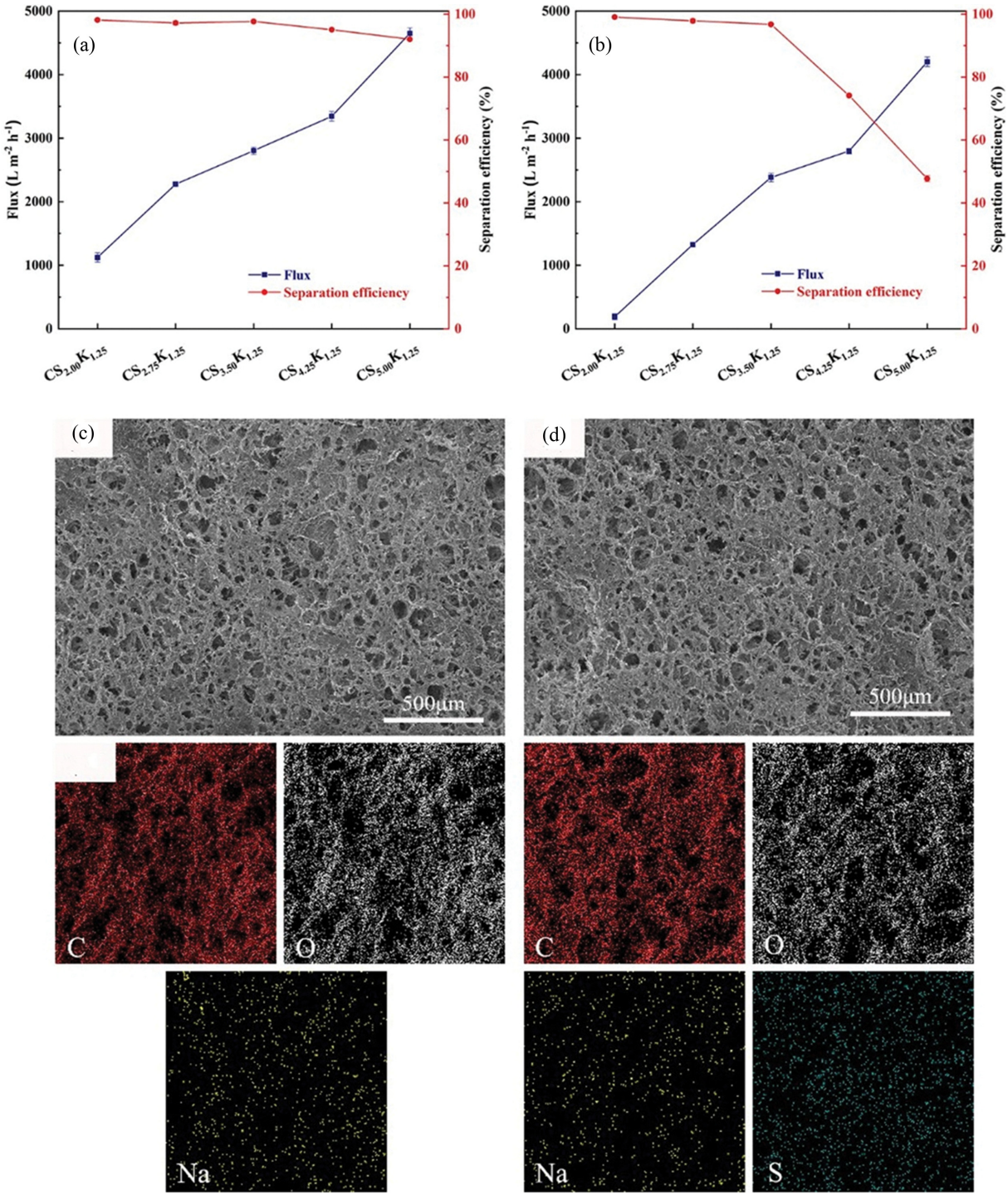

Fig. 8. Separation performance of CS/KGM aerogel with different CS content for oil-in-water emulsion ((a) surfactant-free emulsion; (b) surfactant-stabilized emulsion.); SEM and EDS mapping of $CS_{3.50}K_{1.25}$ after separation ((c) surfactant-free oil/water emulsion; (d) surfactant-stabilized oil/water emulsion).

CS content increased (Fig. 8(a)). Compared with the surfactant-free oil/water emulsion, the flux of the aerogel for surfactant-stabilized oil/water emulsion declined (Fig. 8(b)). This is due to the interaction between SDS and the hydroxyl groups on the aerogel surface, and the porous structure of CS/KGM aerogels was fouled and clogged by the surfactant and absorbed species, resulting in the decrease of permeability [53,59]. Fig. 8(d) is the EDS mapping of $CS_{3.50}K_{1.25}$ after the separation of surfactant-stabilized oil/water emulsion. It is obvious that S element exists on the surface of CS/KGM aerogels. This result indicates that the aerogel was fouled by the surfactant in the separation process of the surfactant-stabilized oil/water emulsion. However, there is no interaction between sur-

Table 1. Comparison of the oil/water emulsion performance with the materials in the literature

Materials	Driver	Flux	Separation efficiency	Ref.
Chitosan-based aerogel	1 bar	650 L m^{-2} h^{-1}	99.00%	[60]
PES/PDA membrane	1 bar	181 L m^{-2} h^{-1}	99.12%	[61]
Cellulose sponge	gravity	91 L m^{-2} h^{-1}	99.94%	[17]
PEI@CNT-TMC membrane	1 bar	2,854 L m^{-2} h^{-1}	81.70%	[62]
PES/PDA/N-MWCNT membrane	1 bar	117 L m^{-2} h^{-1}	99.13%	[63]
CS3.50K1.25	0.9 bar	2,381 L m^{-2} h^{-1}	96.26%	This work

factants and CS/KGM aerogels for the surfactant-free emulsion. So, the flux of the aerogel for surfactant-stabilized emulsion is lower than the surfactant-free emulsion.

There is a trade-off between flux and separation efficiency as the porous structure of the superhydrophilic aerogel changes [19]. The incorporation of CS is beneficial to increasing the flux, but a relatively high flux is not favorable to the emulsion interacting with the hydrophilic groups on the aerogel surface for demulsification. So the separation efficiency decreased slightly with the CS content increased (≤3.50%). However, the separation efficiency reduced greatly with the CS content increased to 4.25%, especially for the surfactant-stabilized emulsion. In our experiment, $CS_{3.50}K_{1.25}$ achieved optimal separation performance with an excellent separation efficiency above 96.26% and a high permeate flux above 2,381 L m^{-2} h^{-1} for emulsions. Compared with those of the advanced oil/water emulsion separation materials reported in the literature (Table 1), $CS_{3.50}K_{1.25}$ showed a slightly lower separation efficiency, but it had a great advantage in permeation flux. These results imply that the $CS_{3.50}K_{1.25}$ has promising features for oil/water emulsion separation.

To further visually elaborate an effective separation for surfactant-stabilized oil-in-water emulsion, optical microscopy and dynamic light scattering (DLS) were used to observe the difference in size distribution of pristine emulsion and the corresponding collected filtrate [64]. As shown in Fig. 9(a), the milky white color pristine emulsion changed to transparent after filtering. By comparing the images of optical microscopy, compact droplets flood can be observed in the pristine emulsion and not any droplets in the filtrate. Furthermore, the DLS data illustrate the results of separation, the size distributions of emulsion droplets was about 0.8 μm to 2.3 μm before separation and no oil droplets in this range were observed in the filtrate. It is noted the oil droplets distributed in the range of 1-2 nm in the filtrate were contributed by the SDS rather than the oil droplets (Fig. 9(b)) [65]. The results strongly demonstrate the great potential of $CS_{3.50}K_{1.25}$ for separation applications of oil-in-

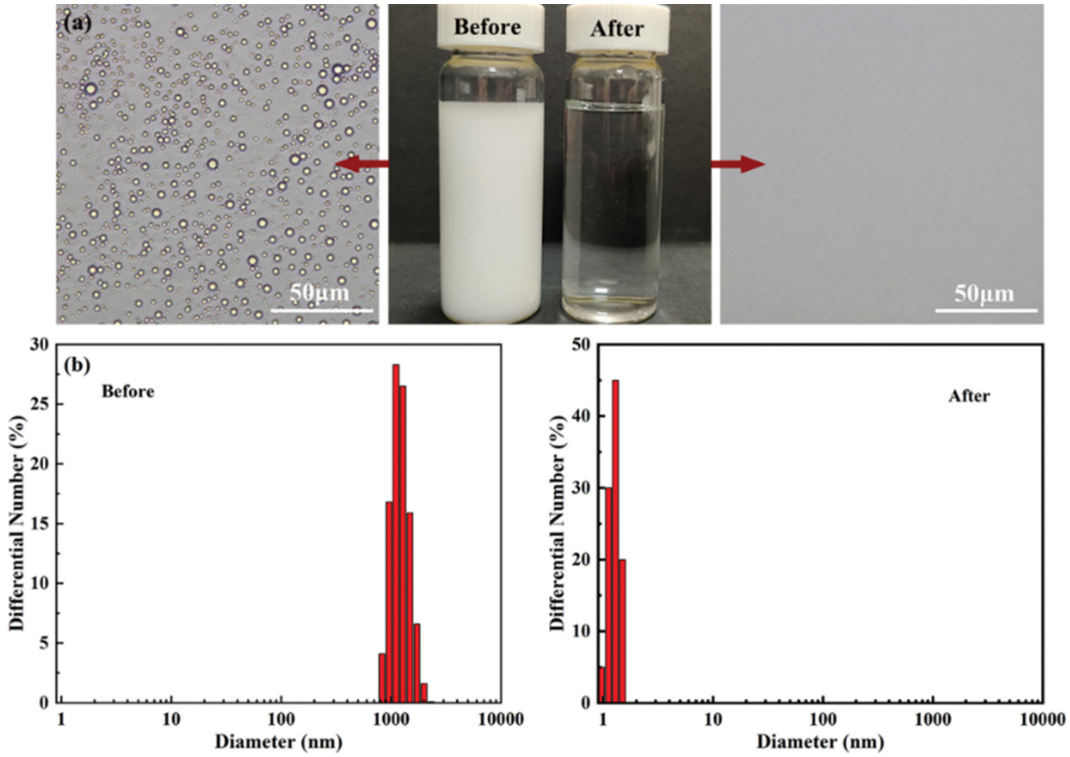

Fig. 9. (a) Digital and optical microscopic photographs of surfactant-stabilized oil-in-water emulsion before and after filtration; (b) DLS data of emulsion before and after filtration.

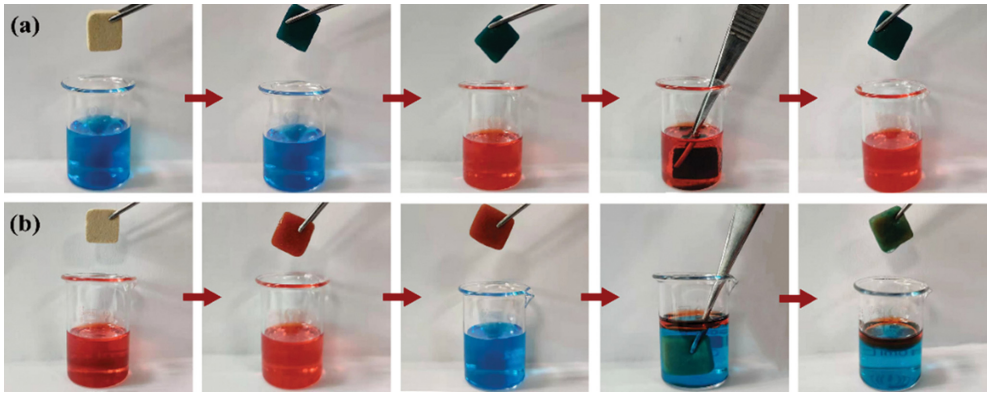

Fig. 10. Digital photograph of (a) underwater anti-oil-fouling and (b) self-cleaning function of $CS_{3.50}K_{1.25}$.

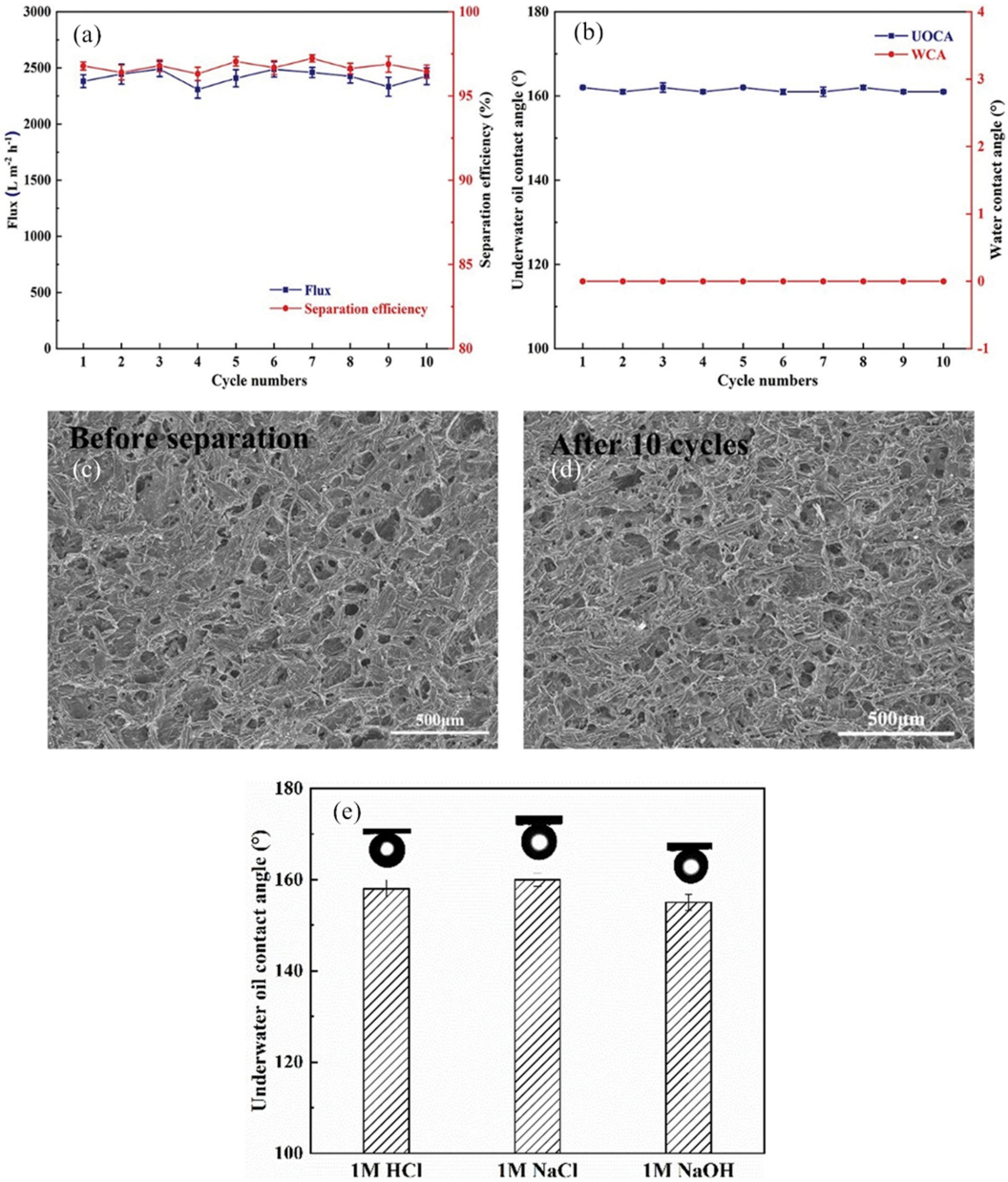

Fig. 11. Separation performance (a), corresponding CA (b) and the stability under harsh chemical conditions (e) of $CS_{3.5}K_{1.25}$ for the separation of surfactant-stabilized oil-in-water emulsion before (c) and after (d) used ten cycles.

water emulsions.

4. Antifouling Property and Recyclability

The anti-oil-fouling and self-cleaning functions of the $CS_{3.50}K_{1.25}$ were realized by the application of underwater superoleophobicity and ultralow oil adhesion [66]. The underwater anti-oil-fouling function of $CS_{3.50}K_{1.25}$ is shown in Fig. 10(a). After being immersed in water (dyed with methylene blue), $CS_{3.50}K_{1.25}$ was wetted quickly by the water and formed a hydration layer between water molecules and hydrophilic groups on the surface of $CS_{3.50}K_{1.25}$ [67]. Subsequently, when the water-wetted $CS_{3.50}K_{1.25}$ was dipped in toluene (dyed with Sudan III), the surface of $CS_{3.50}K_{1.25}$ could not be contaminated by oil for its ultralow oil adhesion [68]. Fig. 10(b) demonstrates the self-cleaning function of $CS_{3.50}K_{1.25}$. The $CS_{3.50}K_{1.25}$ was first dipped in toluene (dyed with Sudan III), such that its surface was contaminated. Subsequently, the contaminated $CS_{3.50}K_{1.25}$ was dipped into water (dyed with methylene blue). As water comes into contact with the $CS_{3.50}K_{1.25}$, the toluene on the surface can be washed rapidly away without leaving any residue. These results consistently implied that the special wettability could effectively prevent the CS/KCM aerogel from being polluted by oils during the oil/water separation process, giving it the possibility of recycling.

To evaluate the recyclability of $CS_{3.50}K_{1.25}$ with antifouling property, ten cycles of filtration were performed. Simultaneously, the underwater oil contact angle of $CS_{3.50}K_{1.25}$ was also recorded for every cycle. Fig. 11(a) shows the flux and separation efficiency versus cycle. There are no obvious changes in the flux (>2,300 L m^{-2} h^{-1}) and separation efficiency (>96%) within ten cycles. The corresponding UWCA (toluene) and WCA are shown in Fig. 11(b). The underwater CA of toluene on $CS_{3.50}K_{1.25}$ were all above 161°, and all water CA were 0°, showing good stability of hydrophilic and underwater superhydrophobic properties. The results indicate that CS/KGM aerogel has excellent durability, which is essential for practical applications.

The change of the aerogel surface after ten cycles was observed by SEM (Fig. 11(d)). After ten cycles, the porous structure of the aerogel surface was maintained constantly, which proved the good stability of the aerogel. This is attributed to the addition of CS improving the structure, porosity and mechanical properties of the aerogel, making it resistant to damage from external mechanical stress during long-term separation. The stability under different chemical conditions was also preliminarily investigated (Fig. 11(e)). The contact angle of the oil droplet remained above 150° in the chemically harsh environments tested, which indicated the stable underwater superoleophobicity of the aerogel even in harsh chemical conditions.

CONCLUSIONS

Combining the benefits of both KGM and CS in a synergistic manner, a novel CS/KGM aerogel with hydrophilicity and underwater superoleophobic was successfully fabricated via a simple way. This special wettability makes it suitable for separating surfactant-free and surfactant-stabilized oil/water emulsions. The obtained aerogel exhibits superior oil/water separation efficiency above 96.26% and a high permeate flux above 2,381 L m^{-2} h^{-1} for oil/water emulsions. The characteristic of hydrophilicity and underwater superoleophobicity endows the CS/KGM aerogel with excellent antifouling property and recyclability, indicating the potential application of the aerogel for separating oily wastewater in industrial contexts. Moreover, CS/KGM aerogel has many advantages, such as biodegradability, low cost and simple preparation. Therefore, it is believed that CS/KGM aerogel has great potential for handling oil-contaminated wastewater.

ACKNOWLEDGEMENTS

The work was supported by the National Key Research and Development Program of China (No. 2019YFC0605003) and the Natural Science Foundation of Liaoning Province (No. 2019-ZD-0293).

CONFLICTS OF INTEREST

There are no conflicts of interest to declare.

REFERENCES

1. J. Cui, A. Xie, S. Zhou, S. Liu, Q. Wang, Y. Wu, M. Meng, J. Lang, Z. Zhou and Y. Yan, *J. Colloid Interface Sci.*, **533**, 278 (2019).
2. Z. Luo, C. Duan, Y. Li, Y. Wang and B. Wang, *RSC Adv.*, **8**, 29570 (2018).
3. J. Dai, R. Zhang, W. Ge, A. Xie, Z. Chang, S. Tian, Z. Zhou and Y. Yan, *Mater. Des.*, **139**, 122 (2018).
4. H. Gong, B. Yu, F. Dai and Y. Peng, *Colloids Surf. A: Physicochem. Eng. Aspects.*, **550**, 27 (2018).
5. R. Etchepare, H. Oliveira, A. Azevedo and J. Rubio, *Sep. Purif. Technol.*, **186**, 326 (2017).
6. U. Rojas-Alva, J. Fritt-Rasmussen and G. Jomaas, *Cold Reg. Sci. Tech.*, **175**, 103083 (2020).
7. M. Karzar Jeddi, O. Laitinen and H. Liimatainen, *Mater. Des.*, **183**, 108 (2019).
8. D. Xu, X. Zheng and R. Xiao, *RSC Adv.*, **7**, 7108 (2017).
9. J. Li, Z. Zhao, Y. Shen, H. Feng, Y. Yang and F. Zha, *Adv. Mater. Interfaces*, **4**, 1700364 (2017).
10. R. D'Apolito, A. Perazzo, M. D'Antuono, V. Preziosi, G. Tomaiuolo, R. Miller and S. Guido, *Langmuir*, **34**, 4991 (2018).
11. X. Zheng, X. Liu and L. Zha, *Macromol. Mater. Eng.*, **304**, 1900125 (2019).
12. F. Crisafi, M. Genovese, F. Smedile, D. Russo, M. Catalfamo, M. Yakimov, L. Giuliano and R. Denaro, *Mar. Pollut. Bull.*, **106**, 119 (2016).
13. M. F. Ismail, B. Khorshidi and M. Sadrzadeh, *J. Membr. Sci.*, **590**, 117270 (2019).
14. M. Zhu, Y. Liu, M. Chen, M. Sadrzadeh, Z. Xu, D. Gan, Z. Huang, L. Ma, B. Yang and Y. Zhou, *J. Membr. Sci.*, **640**, 119755 (2021).
15. S. Zarghami, T. Mohammadi, M. Sadrzadeh and B. Van der Bruggen, *Prog. Polym. Sci.*, **98**, 101166 (2019).
16. X. Yue, T. Zhang, D. Yang, F. Qiu and Z. Li, *Chem. Eng. Sci.*, **203**, 237 (2019).
17. G. Wang, Y. He, H. Wang, L. Zhang, Q. Yu, S. Peng, X. Wu, T. Ren, Z. Zeng and Q. Xue, *Green Chem.*, **17**, 3093 (2015).
18. H. Peng, J. Wu, Y. Wang, H. Wang, Z. Liu, Y. Shi and X. Guo, *Appl.*

Phys. A, **122**, 516 (2016).
19. Z. He, X. Zhang and W. Batchelor, *RSC Adv.*, **6**, 21435 (2016).
20. H. Zhang, Y. Li, R. Shi, L. Chen and M. Fan, *Carbohydr. Polym.*, **200**, 611 (2018).
21. S. S. Behera and R. C. Ray, *Int. J. Biol. Macromol.*, **92**, 942 (2016).
22. G. M. Genevro, M. A. de Moraes and M. M. Beppu, *Int. J. Biol. Macromol.*, **128**, 401 (2019).
23. R.-J. Mu, L. Wang, Y. Du, Y. Yuan, Y. Ni, C. Wu and J. Pang, *Mater. Lett.*, **226**, 75 (2018).
24. J. Zhu, J. Hu, C. Jiang, S. Liu and Y. Li, *Carbohydr. Polym.*, **207**, 246 (2019).
25. Y. Si, X. Wang, C. Yan, L. Yang, J. Yu and B. Ding, *Adv. Mater.*, **28**, 9512 (2016).
26. Q. Jiang, Z. Lin, B. Gu, C. Pang and X. Wang, *Ind. Crops Prod.*, **158**, 112987 (2020).
27. Y. Wang, X. Chen, Y. Kuang, M. Xiao, Y. Su and F. Jiang, *Int. J. Low-Carbon Tech.*, **14**, 335 (2019).
28. T. Y. Chong, M. C. Law and Y. S. Chan, *J. Polym. Environ.*, **29**, 363 (2020).
29. Y. Liu, J. Xie, N. Wu, Y. Ma, C. Menon and J. Tong, *Cellulose*, **26**, 4707 (2019).
30. Q. Jiang, B. Luo, Z. Wu, B. Gu, C. Xu, X. Li and X. Wang, *Chem. Eng. J.*, **421**, 129815 (2021).
31. Y. Wang, K. Wu, M. Xiao, S.-B. Riffat, Y. Su and F. Jiang, *Carbohydr. Polym.*, **197**, 284 (2018).
32. J.-B. Fan, Y. Song, S. Wang, J. Meng, G. Yang, X. Guo, L. Feng and L. Jiang, *Adv. Funct. Mater.*, **25**, 5368 (2015).
33. C. Qi, C. Luo, Y. Tao, W. Lv, C. Zhang, Y. Deng, H. Li, J. Han, G. Ling and Q.-H. Yang, *Sci. China Mater.*, **63**, 1870 (2019).
34. J. Chen, Y. Zou, H. Ge, Z. Cui and S. Liu, *J. Appl. Polym. Sci.*, **135**, 46405 (2018).
35. D. Qiao, J. Lu, W. Shi, H. Li, L. Zhang, F. Jiang and B. Zhang, *Carbohydr. Polym.*, **276**, 118776 (2022).
36. X. Li, F. Jiang, X. Ni, W. Yan, Y. Fang, H. Corke and M. Xiao, *Food Hydrocolloids*, **44**, 229 (2015).
37. X. Ye, J. F. Kennedy, B. Li and B.-J. Xie, *Carbohydr. Polym.*, **64**, 532 (2006).
38. W. Jin, R. Song, W. Xu, Y. Wang, J. Li, B. R. Shah, Y. Li and B. Li, *Food Hydrocolloids*, **48**, 320 (2015).
39. J. Liu, B. Li, B. Zhu, R.-H. Fu, L.-N. Yuan, W. Huang and M.-H. Ma, *J. Appl. Polym. Sci.*, **115**, 1503 (2010).
40. H. Li, X. Chen, J. Ren, H. Deng, F. Peng and R. Sun, *Biotechnol. Biofuels*, **8**, 127 (2015).
41. L. Wang, R.-J. Mu, L. Lin, X. Chen, S. Lin, Q. Ye and J. Pang, *Int. J. Biol. Macromol.*, **133**, 693 (2019).
42. Z. Wu, C. Tong, J. Zhang, J. Sun, H. Jiang, M. Duan, C. Wen, C. Wu and J. Pang, *Int. J. Biol. Macromol.*, **192**, 323 (2021).
43. E. Kamelnia, A. Divsalar, M. Darroudi, P. Yaghmaei and K. Sadri, *Int. J. Biol. Macromol.*, **146**, 299 (2020).
44. J. Cui, Q. Wang, A. Xie, J. Lang, Z. Zhou and Y. Yan, *J. Taiwan Inst. Chem. Eng.*, **104**, 240 (2019).
45. C. Guan, Z. Li, L. Zhu and D. Xia, *Sep. Purif. Technol.*, **269**, 118715 (2021).
46. A. Bajpayee, T. E. G. Alivio, P. McKay and S. Banerjee, *Energy Fuels*, **33**, 5024 (2019).
47. M. Wang, Z. Xu, Y. Hou, P. Li, H. Sun and Q.-J. Niu, *Sep. Purif. Technol.*, **251**, 117408 (2020).
48. M. F. Ismail, M. A. Islam, B. Khorshidi, A. Tehrani-Bagha and M. Sadrzadeh, *Adv. Colloid Interface Sci.*, **299**, 102524 (2022).
49. X. Zeng, J. Lin, W. Cai, Q. Lu, S. Fu, J. Li, X. Yan, X. Wen, C. Zhou and M. Zhang, *Chemosphere*, **264**, 128395 (2021).
50. J. Ge, D. Zong, Q. Jin, J. Yu and B. Ding, *Adv. Funct. Mater.*, **28**, 1705051 (2018).
51. X. You, Y. Liao, M. Tian, J. W. Chew and R. Wang, *J. Membr. Sci.*, **611**, 118398 (2020).
52. B. He, Y. Ding, J. Wang, Z. Yao, W. Qing, Y. Zhang, F. Liu and C.-Y. Tang, *J. Membr. Sci.*, **581**, 105 (2019).
53. G. Zhang, L. Li, Y. Huang, A. Hozumi, T. Sonoda and Z. Su, *RSC Adv.*, **8**, 5306 (2018).
54. C. Xu, F. Yan, M. Wang, H. Yan, Z. Cui, J. Li and B. He, *J. Membr. Sci.*, **602**, 117974 (2020).
55. S. Ma, L. Lin, Q. Wang, Y. Zhang, H. Zhang, Y. Gao, F. Pan and Y. Zhang, *J. Membr. Sci.*, **595**, 117562 (2020).
56. Y. Gu, B. Zhang, Z. Fu, J. Li, M. Yu, L. Li and J. Li, *J. Membr. Sci.*, **619**, 118792 (2021).
57. X. Shen, P. Liu, C. He, S. Xia, J. Liu, F. Cheng, H. Suo, Y. Zhao and L. Chen, *Sep. Purif. Technol.*, **255**, 117418 (2021).
58. W. Wang, Y. Fang, X. Ni, K. Wu, Y. Wang, F. Jiang and S. B. Riffat, *Carbohydr. Polym.*, **224**, 115129 (2019).
59. R. Zhang, Y. Liu, M. He, Y. Su, X. Zhao, M. Elimelech and Z. Jiang, *Chem. Soc. Rev.*, **45**, 5888 (2016).
60. J. P. Chaudhary, N. Vadodariya, S. K. Nataraj and R. Meena, *ACS Appl. Mater. Interfaces*, **7**, 24957 (2015).
61. S. Zarghami, T. Mohammadi and M. Sadrzadeh, *J. Membr. Sci.*, **582**, 402 (2019).
62. Y. Liu, Y. Su, J. Guan, J. Cao, R. Zhang, M. He and Z. Jiang, *ACS Appl. Mater. Interfaces*, **10**, 26546 (2018).
63. S. Zarghami, T. Mohammadi, M. Sadrzadeh and B. Van der Bruggen, *Sci. Total Environ.*, **711**, 134951 (2020).
64. Y. Deng, G. Zhang, R. Bai, S. Shen, X. Zhou and I. Wyman, *J. Membr. Sci.*, **569**, 60 (2019).
65. S. Gao, Y. Zhu, J. Wang, F. Zhang, J. Li and J. Jin, *Adv. Funct. Mater.*, **28**, 1801944 (2018).
66. Y. Wang, Y. He, S. Yan, X. Yin and J. Chen, *Colloids Surf. A: Physicochem. Eng. Aspects.*, **582**, 123891 (2019).
67. K. Venkatesh, G. Arthanareeswaran, A. C. Bose and P. S. Kumar, *Sep. Purif. Technol.*, **241**, 116709 (2020).
68. Y. Du, Y. Li and T. Wu, *RSC Adv.*, **7**, 41838 (2017).